

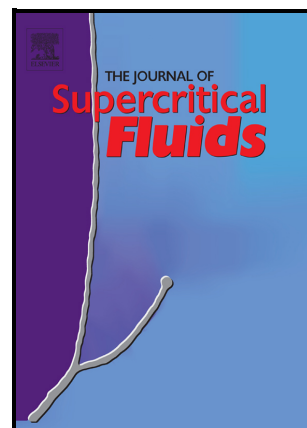
ULRR

Solubility of naproxen and indomethacin in supercritical carbon dioxide/ethyl acetate mixtures

Item Type	Article
Authors	Petza Kloc, Amábille;Danzer, Andreas;Sadowski, Gabriele
Citation	The Journal of Supercritical Fluids, 2023, 105990
Publisher	Elsevier
Download date	2026-05-14 01:39:39
Item License	https://creativecommons.org/licenses/by-nc-sa/4.0/
Link to Item	https://doi.org/10.34961/researchrepository-ul.26537818

Solubility of Naproxen and Indomethacin in Supercritical Carbon Dioxide/Ethyl Acetate Mixtures

Amáville Petza Kloc, Andreas Danzer, Gabriele Sadowski



PII: S0896-8446(23)00154-7

DOI: <https://doi.org/10.1016/j.supflu.2023.105990>

Reference: SUPFLU105990

To appear in: *The Journal of Supercritical Fluids*

Received date: 20 February 2023

Revised date: 26 April 2023

Accepted date: 15 May 2023

Please cite this article as: Amáville Petza Kloc, Andreas Danzer and Gabriele Sadowski, Solubility of Naproxen and Indomethacin in Supercritical Carbon Dioxide/Ethyl Acetate Mixtures, *The Journal of Supercritical Fluids*, (2023) doi:<https://doi.org/10.1016/j.supflu.2023.105990>

This is a PDF file of an article that has undergone enhancements after acceptance, such as the addition of a cover page and metadata, and formatting for readability, but it is not yet the definitive version of record. This version will undergo additional copyediting, typesetting and review before it is published in its final form, but we are providing this version to give early visibility of the article. Please note that, during the production process, errors may be discovered which could affect the content, and all legal disclaimers that apply to the journal pertain.

© 2023 Published by Elsevier.

Solubility of Naproxen and Indomethacin in Supercritical Carbon Dioxide/Ethyl Acetate Mixtures

*Amáville Petza Kloc, Andreas Danzer, and Gabriele Sadowski**

TU Dortmund University, Department of Biochemical and Chemical Engineering, Laboratory of Thermodynamics, Emil-Figge-Str. 70, D-44227 Dortmund, Germany

Abstract

In this work, the solubilities of naproxen and indomethacin in supercritical carbon dioxide (scCO₂) were investigated from both experimental and theoretical points of view. Experimentally, the solubilities of those active pharmaceutical ingredients (APIs) in scCO₂ and scCO₂/ethyl acetate were measured using a variable-volume high-pressure view cell at T = 60 °C and pressures between 150 and 429 bar. Results showed two different trends for the solubility of naproxen in scCO₂ and further PXRD analysis revealed a change in naproxen crystal structure for pressures above 250 bar. Moreover, the influence of ethyl acetate on the solubility of indomethacin in scCO₂ was investigated. At constant pressure, solubility was observed to increase with increasing ethyl acetate concentration. PC-SAFT was used to describe the solubility of both APIs in scCO₂ and of indomethacin in the scCO₂/ethyl acetate mixture over the entire pressure range. The melting properties of different polymorphic forms were considered for the solubility calculations, and the model accurately described the investigated systems.

Keywords: solid-fluid equilibrium, supercritical carbon dioxide, naproxen, indomethacin, PC-SAFT.

1. Introduction

Most of the active pharmaceutical ingredients (APIs) have a very low solubility in water, thus leading to poor bioavailability when administered through oral delivery [1]. Increasing the API surface area by particle-size reduction can enhance the API dissolution behavior, therewith increasing its bioavailability [2,3]. Techniques for particle-size reduction using a supercritical fluid, like supercritical antisolvent precipitation (SAS) and gas antisolvent precipitation (GAS), often apply supercritical carbon dioxide (scCO₂) as antisolvent, since it is nonflammable, nontoxic, inexpensive and presents low critical properties ($T_c = 31\text{ °C}$ and $p_c = 73.8\text{ bar}$) [4]. These techniques are usually performed by mixing an API solution in an organic solvent with a supercritical fluid, followed by expansion. The mixture density dramatically decreases during expansion, leading to high supersaturation and, therefore, high nucleation rates and crystal-growth rates. This process results mainly in an uniform crystal growth of the particles, enabling the formation of particles in the nano scale [5]. Moreover, the nucleation rate is a function of supersaturation and interfacial tension [6], thus the API solubility in pure scCO₂ and in scCO₂/organic solvent mixtures is an important property to be investigated.

Different authors investigated the solubility of naproxen in supercritical CO₂ at experimental conditions varying between 298.15 – 353 K and 89 – 400 bar. Ting et al. used a flow technique to allow the contact between solid and supercritical phases and let them equilibrate at constant temperature and pressure for several hours. Upon decreasing pressure, naproxen precipitated due to the supersaturation at lower pressures. The amount of naproxen which was dissolved in scCO₂ was measured gravimetrically by weighing the precipitated naproxen [7]. Garmroodi et al. investigated the solubility of naproxen in scCO₂ using supercritical fluid extraction (SFE)/supercritical fluid chromatography (SFC) combined with UV-Vis spectrophotometer

analysis [8]. Suleiman et al. measured the solubility of naproxen in scCO₂ using a chromatographic method coupled with a dynamic solubility apparatus [9].

Türk and Kraska used a static method coupled with gravimetric analysis to determine the solubility of naproxen in scCO₂. In this technique, a vial with a known amount of naproxen was placed into a high-pressure cell, followed by a known amount of carbon dioxide. The system was allowed to equilibrate for minimum 12 h. The cell was then depressurized, and the vial was reweighed to calculate the mass of naproxen that was dissolved in scCO₂ [4]. Revelli et al. developed a new analytical method for measuring the solubility of APIs in supercritical fluid using a variable-volume cell with sampling of the supercritical-fluid phase for HPLC analysis [10]. The solubility of indomethacin in supercritical CO₂ was reported once by the group of Padrela et al. The authors used a variable-volume high-pressure cell to measure the mentioned indomethacin solubility in scCO₂ at 30°C and 50°C and in pressure range between 80 and 200 bar [11].

The before-mentioned publications reported a strong influence of system temperature and of scCO₂ density on API solubility. Higher API solubilities were achieved at higher pressures, due to an increase in scCO₂ solvent strength caused by the density increase [4,7–10]. The addition of organic co-solvents was found to increase the solubility of naproxen in scCO₂ due to density increase and specific interactions with the API [7,10]. However, none of the above-mentioned publications investigated the presence of polymorphs.

Polymorphism refers to the appearance of different crystal structures for the same component. From the thermodynamic perspective, the stable crystal structure is the one with the lowest free energy [12]. Naproxen is reported to have four different polymorphic forms, being form 1 the thermodynamically most stable one [13]. Indomethacin presents two main

polymorphic forms (α and γ), with γ being the thermodynamically stable form, and α being the most common metastable form [14,15]. It is vastly reported in literature that experimental conditions like temperature and solvent choice have an influence on solvate formation and/or polymorphic transformation of an API [16–19].

However, the influence of system pressure on polymorphic transformation and solvate formation of indomethacin has been scarcely reported in literature. Okumura et al. investigated the influence of pressure on the polymorphic transformation of indomethacin and reported that the formation of α -indomethacin is favored under higher pressures due to its higher density compared to the γ -form [20]. Despite the fact that investigating the pressure influence on polymorphic transformation of indomethacin was not the main research focus so far, a change from the γ -form to the α -form after indomethacin crystallization using supercritical CO₂ has been reported in literature [21–24]. Kim and Yeo investigated the crystallization of indomethacin by injecting scCO₂ into a chamber containing an undersaturated acetone/API solution, at temperatures between 25-45°C and $p = 95$ bar. Further solid form analysis revealed the precipitate to be a mixture of both α - and γ - polymorphic forms [21]. The precipitation of both polymorphic forms can be attributed to the difference between their surface energies, thus in their nucleation rates, causing a mixture of α -indomethacin and γ -indomethacin to precipitate. Varughese et al. processed indomethacin with a supercritical antisolvent (SAS) technique [22]. The API was precipitated from solutions of acetone, dichloromethane and dimethylsulfoxide, in temperature and pressure ranges of 35-55°C and 83-117 bar, respectively, and the authors consistently obtained the α -polymorph [22]. The research group of Tozuka promoted the crystallization of indomethacin from an ethanol solution by combining supercritical antisolvent precipitation and rapid expansion from supercritical to aqueous solution (RESAS) techniques

and obtained α -indomethacin for the samples treated at 40°C and 100 bar [23]. Rodrigues and coworkers compared the polymorphic forms obtained when processing indomethacin with two different antisolvent precipitation techniques: atomization of supercritical antisolvent induced suspension (ASAIS) and supercritical enhanced atomization (SEA). The experiments were performed at the same temperature (50°C) and pressure (90 bar) and for both techniques the authors observed a transformation from γ - indomethacin to α -indomethacin to be induced by atomization [24]. It is important to note that for all the mentioned supercritical antisolvent experiments the authors started with γ -indomethacin powder.

In this work, the solubilities of naproxen (NAP) in $scCO_2$ and of indomethacin (IND) in $scCO_2$ and in ethyl acetate/ $scCO_2$ mixtures will be discussed from theoretical and experimental perspectives. The solid-fluid equilibrium was calculated using a solubility equation which enables solubility calculations for the entire pressure range as presented by Seiler et al. [25]. The non-ideality of the supercritical phase was described using the thermodynamic model PC-SAFT. Moreover, the formation of different polymorphs under system conditions was investigated, and phase diagrams considering the melting properties of each polymorph are presented. To compare the PC-SAFT descriptions to experimental data, a high-pressure variable-volume view cell is used to investigate the solubilities of the mentioned APIs from the experimental perspective.

2. Modeling

2.1. Phase Equilibria

2.1.1. Gas-liquid equilibrium (GLE)

The GLE of a system containing i components was modeled for all components according to Eq.s (1 – 2), with Eq. 2 being the isofugacity criteria. In this work, the GLE between scCO₂ and ethyl acetate (EtOAc) was calculated.

$$p^L(T, \rho^L, x_i^L) = p^G(T, \rho^G, x_i^G) \quad (1)$$

$$x_i^L \varphi_i^L(T, \rho^L, x_i^L) = x_i^G \varphi_i^G(T, \rho^G, x_i^G) \quad (2)$$

p refers to system pressure, T denotes the temperature, and the superscripts L and G refer to the liquid and gas phases, respectively. φ_i refers to the fugacity coefficient of component i , x_i is the mole fraction of component i , and ρ is the density of the respective phases. In this work, the fugacity coefficients were obtained from the thermodynamic model PC-SAFT.

2.1.2. Solid-fluid Equilibrium (SFE)

The solubility of NAP and IND in scCO₂ and in scCO₂/EtOAc mixtures was modeled as solid-fluid equilibrium. Assuming a pure solid phase, the solubility of an API in the supercritical (fluid) phase (x_{API}^F) at different pressures was calculated according to Eq. (3), as described previously by Seiler and coworkers [25].

$$x_{API}^F = \frac{\varphi_{0,API}^F}{\varphi_{API}^F} \exp \left\{ - \frac{(v_{0,API}^S - v_{0,API}^L)(p^+ - p)}{RT} - \frac{\Delta h_{API}^{SL}}{RT} \left(1 - \frac{T}{T_{API}^{SL}} \right) - \frac{\Delta c_{p,API}^{SL}}{R} \left[\ln \left(\frac{T_{API}^{SL}}{T} \right) - \frac{T_{API}^{SL}}{T} + 1 \right] \right\} \quad (3)$$

Here, R is the universal gas constant, $T_{\text{API}}^{\text{SL}}$ is the API melting temperature, $\Delta h_{\text{API}}^{\text{SL}}$ is the API melting enthalpy, $\Delta c_{\text{p,API}}^{\text{SL}}$ is the difference between the API solid and liquid isobaric heat capacities, $v_{0,\text{API}}^{\text{S}}$ is the molar volume of the pure solid API, $v_{0,\text{API}}^{\text{L}}$ is the molar volume of the pure liquid API at the solid-liquid transition. The before-mentioned properties refer to the standard pressure $p^+ = 1$ bar. The same approach was followed by Seiler et al. to calculate the solubility of naphthalene in scCO_2 . These authors reported a good agreement between the experimental data and calculated results [25].

The fugacity coefficients of the pure API and of the API in the fluid phase ($\phi_{0,\text{API}}^{\text{F}}$ and $\phi_{\text{API}}^{\text{F}}$, respectively) and the molar liquid volume of the API at the solid-liquid transition ($v_{0,\text{API}}^{\text{L}}$) present in Eq.3 were described by PC-SAFT. It is important to note, that polymorphic forms of the same API only differ on their melting properties, as shown in Table 1. Thus, the fugacity coefficients of different polymorphic forms in a fluid phase are identical. The molar liquid volume of the API at the melting temperature, however, does depend on the polymorph since the melting temperatures of the polymorphs differ. The molar volume of the solid API ($v_{0,\text{API}}^{\text{S}}$) also depends on the API solid form and was fitted to experimental solubility data obtained in this work.

Table 1. Melting properties of crystal forms investigated in this work.

Substance	Crystal form	$T_{\text{API}}^{\text{SL}}$ [K]	$\Delta h_{\text{API}}^{\text{SL}}$ [kJ mol ⁻¹]	$\Delta c_{\text{p,API}}^{\text{SL}}$ [J mol ⁻¹ K ⁻¹]	Ref
NAP	1	429.47	31.5	87.44	[26]
NAP	3	413.15	21.9	87.44	[13,26]
IND	α	424.55	37.03	116.95	[17]
Naphthalene	-	353.43	18.98	8.8	[27]

2.2. Perturbed-Chain Statistical Associating Fluid Theory

The vapor pressure of the organic solvent, the fugacity coefficients accounting for the non-ideality of the fluid phase and the API molar liquid volumes were obtained in this work from PC-SAFT. Developed by Gross and Sadowski, this thermodynamic model calculates thermodynamic properties of pure components and mixtures based on the residual Helmholtz energy (a^{res}). The latter is obtained as a sum of different molecular contributions, namely hard chain repulsion (a^{hc}), van der Waals dispersion (a^{disp}), and hydrogen bonding (a^{assoc}), as described in Eq. (4) [28].

$$a^{\text{res}} = a^{\text{hc}} + a^{\text{disp}} + a^{\text{assoc}} \quad (4)$$

Each component is described by at least three pure-component parameters: the number of spherical segments (m^{seg}), the segment diameter σ , and the dispersion-energy parameter (u_i/k_B), where k_B is the Boltzmann constant. Two additional parameters, the association-energy parameter ($\epsilon^{A_i B_i}/k_B$) and the association volume ($\kappa^{A_i B_i}$), are required for associating molecules, e. g. molecules that form hydrogen bonds.

For binary mixtures of components i and j , the segment diameter (Eq. 5) and the dispersion-energy parameter (Eq. 6) are obtained by the combining rules of Berthelot-Lorentz. The combining rules of Wolbach and Sandler [29] are used to calculate the association-energy parameter $\epsilon^{A_i B_j}/k_B$ (Eq. 7) and the association volume $\kappa^{A_i B_j}$ (Eq. 8) of the binary mixture.

$$\sigma_{ij} = \frac{1}{2}(\sigma_i + \sigma_j) \quad (5)$$

$$u_{ij} = \sqrt{u_i u_j}(1 - k_{ij}) \quad (6)$$

$$\epsilon^{A_i B_j} = \frac{1}{2} (\epsilon^{A_i B_i} + \epsilon^{A_j B_j}) \quad (7)$$

$$\kappa^{A_i B_j} = \sqrt{\kappa^{A_i B_i} \kappa^{A_j B_j}} \left(\frac{\sqrt{\sigma_i \sigma_j}}{\left(\frac{1}{2} (\sigma_i + \sigma_j) \right)} \right)^3 \quad (8)$$

In Eq. 6, deviations of the dispersion energy between unlike segments can be corrected by fitting the binary interaction parameter k_{ij} to experimental data. In this work, k_{ij} was assumed to be constant and was fitted to solubility data. The average absolute deviation (AAD) and maximum absolute deviation (MAD) were calculated to evaluate the model accuracy (Eq. 9-10).

$$\text{AAD} = \frac{1}{n_{\text{exp}}} \sum_{i=1}^{n_{\text{exp}}} |w_{\text{calc},i} - w_{\text{exp},i}| \quad (9)$$

$$\text{MAD} = \max_{i=1, n_{\text{exp}}} |w_{\text{calc},i} - w_{\text{exp},i}| \quad (10)$$

where $w_{\text{calc},i}$ and $w_{\text{exp},i}$ refer to modelled and measured solubilities, respectively, and n_{exp} is the number of experimental points.

PC-SAFT pure-component parameters of all components investigated in this work were taken from literature and are summarized in Table 2. All k_{ij} values fitted in this work and corresponding AAD and MAD values are presented in Table 3. The k_{ij} between IND and EtOAc was fitted to the ternary system α -IND/EtOAc/scCO₂. The molar liquid volumes of the pure APIs predicted by PC-SAFT and their molar solid volumes adjusted to experimental data are presented in Table 4. It is important to note that the APIs pure-component parameters and the binary interaction parameters do not depend on the API polymorphic form, as they are not related to the solid state but only to the liquid/supercritical state of the compound.

Table 2. Molar mass and PC-SAFT pure-component parameters of components investigated in this work.

Substance	M (g/mol)	m_i^{seg} (-)	σ_i (Å)	u_i/k_B (K)	$\epsilon^{A_i B_i}/k_B$ (K)	$\kappa^{A_i B_i}$ (-)	N_i^{assoc} (-)	Ref.
CO ₂	44.01	2.0729	2.7852	169.21	0	0	-	[28]
EtOAc	88.106	3.5375	3.3079	230.80	0	0	-	[28]
IND	357.79	14.283	3.535	262.79	886.4	0.02	3/3	[30]
NAP	230.26	8.1051	2.939	229.450	934.2	0.02	2/2	[30]
Naphthalene	128.17	3.0047	3.9133	353.63	0	0	-	[31]

Table 3. Binary PC-SAFT interactions parameters used in this work.

System	k_{ij}	Ref.	AAD (-)	MAD
NAP/CO ₂	0.257	This work	1.2×10^{-5}	2.2×10^{-5}
IND/CO ₂	0.073	This work	9.1×10^{-7}	2.6×10^{-6}
IND/EtOAc	0.0475	This work	-	-
Naphthalene/CO ₂	0.121	This work	2.1×10^{-3}	8.1×10^{-3}
CO ₂ /EtOAc	0.03	[32]	1.3×10^{-2}	3.6×10^{-2}

Table 4. Molar liquid volumes at the melting temperature (predicted by PC-SAFT) and molar solid volumes (fitted to experimental data obtained in this work).

Substance	Crystal form	$v_{0,API}^L$ (cm ³ /mol)	$v_{0,API}^S$ (cm ³ /mol)
NAP	1	171.86	520
NAP	3	168.68	385
IND	α	482.88	290
Naphthalene	-	131.98	99

3. Experimental section

3.1. Materials

All chemicals used in this work, their purity and suppliers, are presented in Table 5. All compounds were used as obtained without further purification.

Table 5. Chemicals used in this work, their purity and suppliers.

Chemical	Purity	Supplier
CO ₂	≥99.9%	Messer Industriegase GmbH
EtOAc	>99.5%	Th. Geyer
IND (γ -form)	>98.0%	Tokyo Chemical Industry
NAP (form 1)	>99.0%	Tokyo Chemical Industry

3.2. Methods

3.2.1. Solubility measurements using a high-pressure apparatus

The solubility measurements of NAP and IND in scCO₂ were conducted in a high-pressure view cell ($p_{\max} = 700$ bar, $T_{\max} = 180$ °C), New Ways of Analytics, Lörrach, Germany) with a variable volume from 30 to 60 mL, previously used in our research group and described by Görnert and Sadowski [33]. Two sapphire windows placed at the front and the back of the cell allowed optical investigation of the phase equilibrium. The front window is fixed whilst the back one is movable by applying pressure through a manual hydraulic press M(O) 189 (Maximator, Zorge, Germany) allowing cloud-point measurements. Temperature was controlled by two heating jackets and measured inside the cell by a Pt-100 thermocouple (STD = 0.1 K).

A known API amount (weighed on an Curbis analytical balance, accuracy ± 0.1 mg) was added to the cell through its front part. In case of the ternary system IND/scCO₂/EtOAc, a defined amount of EtOAc was added after the API. The cell was completely closed, and a defined volume of CO₂ was added into the cell using a 260D syringe pump ($p_{\max} = 560$ bar, ISCO, Lincoln, New England) at constant temperature and pressure. The system was then homogenized by a magnetically coupled stirrer. The pressure was increased by means of a manual hydraulic press to obtain a homogeneous phase, and then decreased with a rate of 1 MPa/min until turbidity was observed. The temperature inside the cell was controlled within ± 1 K and remained constant even with fast depressurization. After the heating was turned off, the cell needed around 3 h to cool down to room temperature. This procedure was repeated at least six times for each solubility point. The turbidity pressure is the pressure required to dissolve the predetermined amount of API in the given amount of CO₂ (and solvent).

3.2.2. PXRD measurements.

After the solubility measurements were performed, the cell was depressurized by opening the CO₂ valve. The cell was then disassembled and the API which remained inside the chamber was collected and submitted to solid form analysis. The solid state of NAP was analyzed with power X-ray diffractometer (Miniflex 600, Rigaku; Ettlingen, Germany). The PXRD was conducted with Cu-K alpha irradiation, with tube voltage of 40 kV and current of 15 mA. The measurements were recorded in the region of $2^\circ \leq 2\theta \leq 35^\circ$ in steps of 0.02° .

3.2.3. Evaluating the effect of pressure on the solid crystal form

In order to evaluate the effect of experimental pressure on the solid transformation of NAP, a qualitative experiment was performed as follows: known amounts of NAP and scCO₂ were added to the high-pressure cell and brought to a constant temperature and pressure in a manner that all the NAP was dissolved. The system was left to equilibrate for at least 12 h at 60 °C and a constant pressure of 250 bar, and then rapidly depressurized. A NAP sample which remained in the cell after depressurization was collected and analyzed via PXRD.

4. Results and Discussion

4.1. Modeling gas-liquid equilibrium using PC-SAFT

The GLE between scCO₂ and EtOAc at 60 °C was described using PC-SAFT by fitting the binary interaction parameter to experimental data from literature, as depicted in Figure 1. PC-SAFT was able to accurately describe the influence of pressure on the phase equilibrium. According to the calculations, the critical pressure of the mixture at 60 °C is in the vicinity of 100 bar. This is a very relevant information, since when measuring solid solubilities in

supercritical fluids/organic solvent mixtures it is necessary to make sure that the system stays above the critical point of the mixture, thus avoiding the appearance of a second fluid phase.

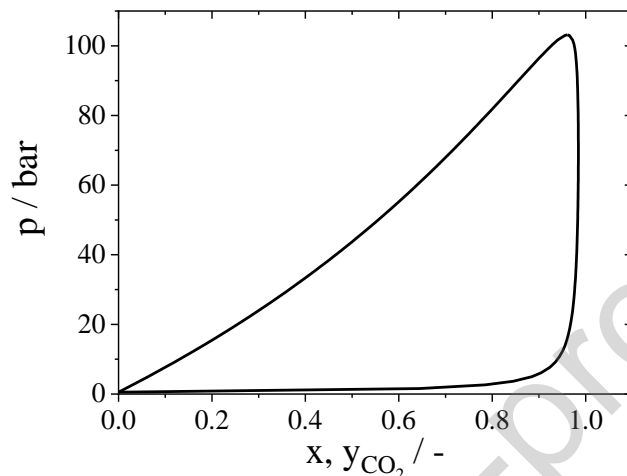


Figure 1. Gas-liquid equilibrium between CO₂/EtOAc at 60 °C. The line represents modeling results using the parameters from Tables 2 and 3. Squares [34], circles [35], and triangles [36] denote experimental data from literature.

4.2. Using PC-SAFT to describe API solubilities in supercritical fluids.

The system naphthalene/scCO₂ was already experimentally investigated in literature. Therefore, it offers the possibility to verify the PC-SAFT accuracy in describing solubilities over a large range of temperatures and pressures in the supercritical regime. The liquid molar volume of naphthalene was calculated using PC-SAFT and the solid molar volume was fitted to experimental data, as for the other systems investigated in this work. The modeling was performed with a temperature-independent k_{ij} (presented in Table 3), and the descriptions were compared to experimental data from literature. The results are presented in Figure 2, showing an AAD and MAD of 0.0021 and 0.0081, respectively.

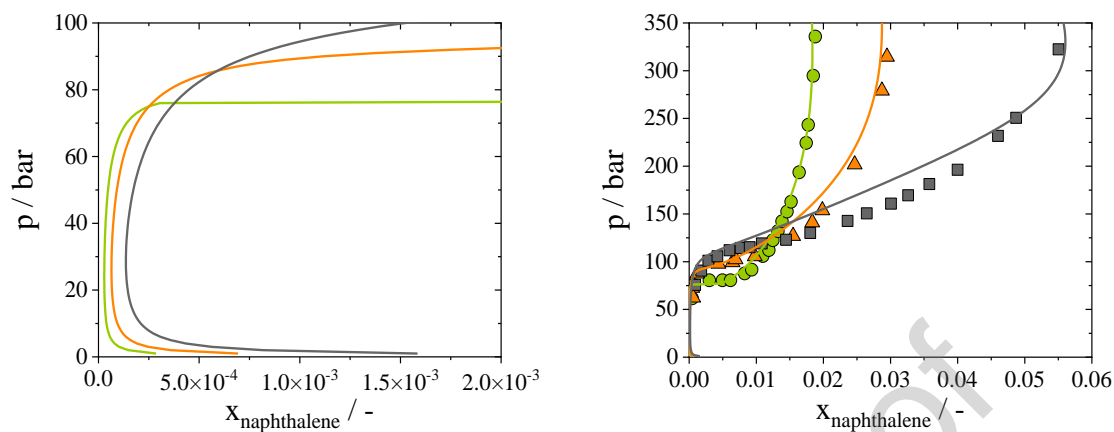


Figure 2. Solubility of naphthalene in $s\text{CO}_2$ at 35°C (green), 45°C (orange), and 55°C (gray). Lines represent PC-SAFT predictions and symbols show experimental data reported in literature [37]. The left diagram represents a zoom in the region up to $x_{\text{naphthalene}} = 2 \times 10^{-3}$.

The left-hand side diagram presented in Figure 2 shows higher solubility values at higher temperatures, for pressures below 70 bar. At constant temperature, the solubility initially decreases with increasing pressure, reaching a minimum, and then rises dramatically. Above a certain pressure, the isotherms intersect. This intersection point is usually called lower crossover pressure. It is around 75 bar for the naphthalene/ $s\text{CO}_2$ system. From this pressure up, it can be observed that solubility decreases with increasing temperature in the region known as retrograde vaporization. The isotherms intersect again at the so-called upper crossover pressure, occurring at around 125 bar for the investigated system. Above the upper crossover pressure, the naphthalene solubility increases with increasing temperature when keeping the pressure constant. The existence of the two crossover pressures as well as the retrograde vaporization region were also previously observed and reported in literature[38–40]. Experimental and predicted crossover pressures of the system naphthalene/ $s\text{CO}_2$ can be clearly observed in Fig. 2, and the model was observed to accurately describe this effect.

This behavior is caused by the opposite temperature influences on both, scCO₂ density (dramatically decreasing with increasing temperature at pressures between about 75 and 125 bar as shown in Fig. 3) and molecular interactions favoring mutual solubility (increasing with increasing temperature). The dramatic density decrease with increasing temperature at pressures between 75 and 125 bar has a bigger effect on the solubility than the increase in attractive molecular interactions leading to an overall solubility decrease in that pressure range. At pressures below 75 bar, the density of scCO₂ becomes quite similar for the different temperatures at and above 125 bar the pressure effect on density diminishes. The same applies to the naphthalene solubility which is obviously mainly determined by the pressure and temperature effect on CO₂ density.

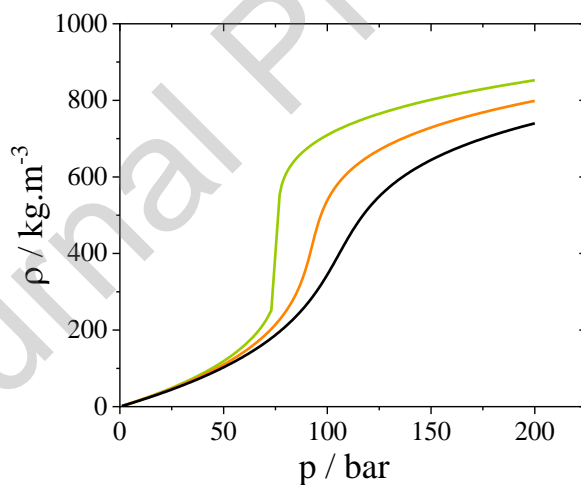


Figure 3. Density of scCO₂ at 35°C (green), 45°C (orange), and 55°C (black) as predicted by PC-SAFT.

4.3. Solubility of NAP in scCO₂

When measuring the solubility of solids in a supercritical fluid, it is important to avoid the formation of additional liquid and/or vapor phases. In order to assure this requirement, a p-T diagram was calculated beforehand to determine optimal experimental conditions, as depicted in

Fig. 4. Above the vapor-pressure curve of CO₂ and left of its critical point only liquid CO₂ (CO₂^L) exist, and below the vapor-pressure curve of naproxen and left of its critical point only vapor naproxen exists (NAP^V). The naproxen melting pressure line starting from the melting point of NAP was calculated using the Clausius-Clapeyron Equation (Eq. 11), where $T_{\text{ref}} = T_{\text{NAP}}^{\text{SL}}$, $p_{\text{ref}} = 1$ bar and assuming that naproxen melting enthalpy and solid molar volume do not depend on temperature nor pressure.

$$p_{\text{API}}^{\text{SL}} = p_{\text{ref}} - \left(\frac{\Delta h_{\text{API}}^{\text{SL}}}{T_{\text{API}}^{\text{SL}} \Delta v_{\text{API}}^{\text{SL}}} (T_{\text{ref}} - T) \right) \quad (11)$$

Here, $T_{\text{API}}^{\text{SL}}$ is the API (NAP) melting temperature, $\Delta h_{\text{API}}^{\text{SL}}$ is the API melting enthalpy and $\Delta v_{\text{API}}^{\text{SL}}$ is the difference between the API solid and liquid molar volumes. The liquid molar volume was predicted by PC-SAFT for $T = T_{\text{ref}}$ using the parameters from Table 2. The solid molar volume was fixed to 178.3 cm³/mol as reported in previous works [4,7].

Right of the melting curve and above the vapor-pressure curve of naproxen, liquid NAP exists (NAP^L). The three-phase solid-liquid-gas (SLG) line of the mixture naproxen/CO₂ was measured experimentally by Türk and Kraska [4]. Only for specific temperature and pressure combinations along the SLG line, the three phases solid, liquid and gas exist simultaneously, where the solid corresponds to pure NAP, and the gas and liquid phases to a mixture of both NAP and CO₂. To the left of the three-phase line, the system is formed by scCO₂ and solid naproxen (NAP^S). Therefore, the target experimental conditions to operate the measurements at $T = 60$ °C were found in the region above the critical temperature of CO₂ and to the left of three-phase line, as indicated in Fig. 4. The critical locus of the mixture as a function of composition

was predicted by PC-SAFT. To the right of this curve both NAP and CO₂ are in the supercritical state.

Different techniques were used in previous works to measure the solubility of NAP in scCO₂, at temperatures ranging from 35 to 80°C, and pressures from 90 to 400 bar [4,7–10]. It is important to note that the NAP polymorphic form before and after the experiments was not reported in the mentioned studies. To validate the experimental method used in this work, the solubility of NAP in scCO₂ at 60°C was measured and compared to results obtained for the same temperature by different authors, as presented in Fig. 5 and Table 6.

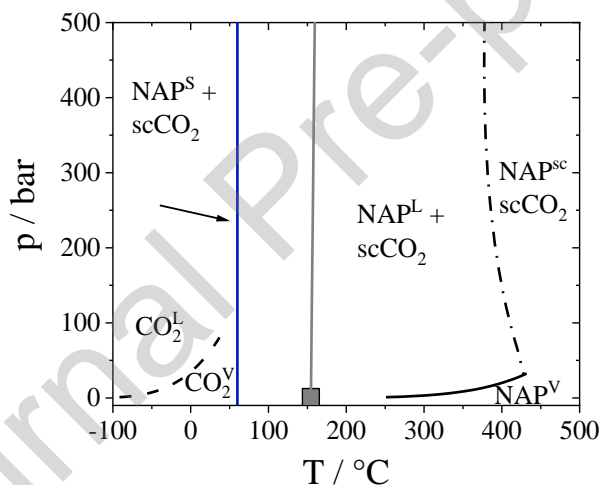


Figure 4. p-T diagram of NAP/CO₂ binary system. Dashed and filled black lines represent the vapor-pressure curves of CO₂ and NAP, respectively, predicted by PC-SAFT. The gray line represents the melting curve of NAP, calculated via the Clausius-Clapeyron equation. Squares represent experimental data of NAP melting temperature (filled square, Ref. [26]) and three-phase solid-liquid-gas data for the binary system NAP/scCO₂ (open squares, Ref. [4]). Dash-dotted line represents the critical locus curve predicted by PC-SAFT. The blue line (indicated by the arrow) depicts conditions at which the experimental measurements in this work were conducted at $T = 60^\circ\text{C}$.

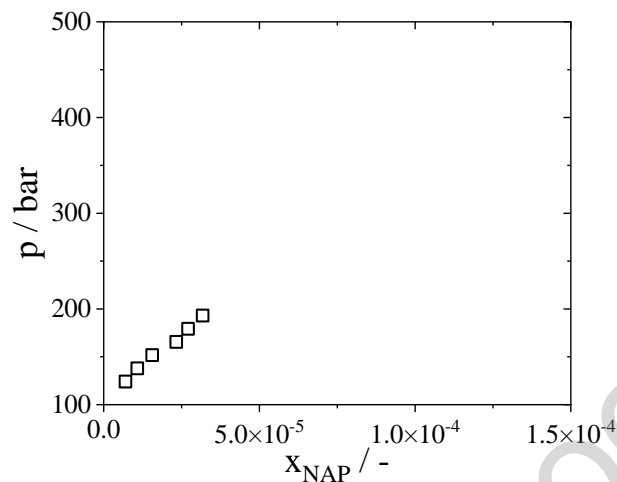


Figure 5. Solubility of NAP in scCO₂ at 60°C. Experimental data are represented by squares [7], triangles [4] and stars (this work).

Table 6. Experimental solubility data NAP obtained in this work for the binary system NAP/scCO₂ at $T = 60$ °C.

$X_{\text{NAP}} / -$	Form	p / bar
2.29×10^{-5}	1	186 ± 2
4.31×10^{-5}	1	217 ± 1
5.55×10^{-5}	1	254 ± 2
1.11×10^{-4}	1	310 ± 3
6.25×10^{-5}	3	377 ± 3
8.75×10^{-5}	3	418 ± 3
1.25×10^{-4}	3	428 ± 3

It can be observed from Fig. 5 that the results obtained in this work agree with the ones reported by Türk and Kaska [4] and Ting et al. [7] up to a pressure of about 250 bar. For pressures higher than 250 bar, two conclusions can be drawn from the diagram: Türk and Kaska reported only one trend in the experimental solubility points above 250 bar, while the

experimental results measured in this work follow two trends, one in agreement with literature data and another one following a different trend. This behavior suggests that solubility data of two different NAP polymorphic forms have been measured in this work.

To verify this assumption, the influence of system pressure on the NAP solid form was evaluated qualitatively as described in the methods section. The PXRD results are shown in Fig. 6. The NAP powder before the experiment was stable form 1. Following the qualitative experimental approach (section 3.2.3), the same form was also obtained at 60°C and 250 bar. However, when the system was exposed to pressures higher than 300 bar in order to dissolve all NAP and perform a cloud-point measurement, a different polymorphic form was obtained. The highest peak that appears at $5 \leq 2\theta \leq 7.5$ corresponds to NAP form 3 as reported by Song and Sohn [13].

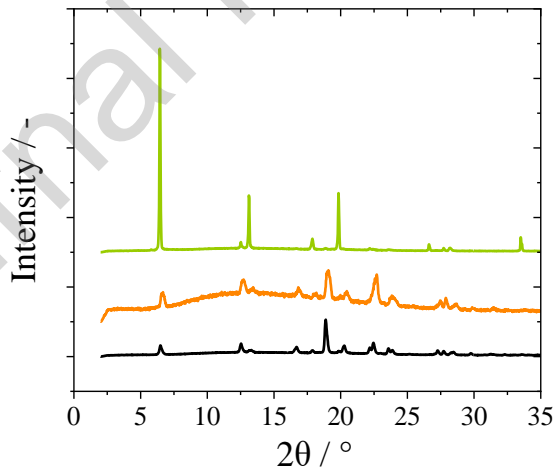


Figure 6. PXRD patterns of NAP. The black line corresponds to the original NAP powder directly from the container. Orange and green lines represent the PXRD pattern obtained after the qualitative approach and cloud-point measurement, respectively.

Changes in the API crystal structure lead to different melting properties as well as heat capacities of the solid and, therefore, to different solubilities. The melting properties of NAP

forms 1 and 3 listed in Table 1 were used to model the solubility of NAP in scCO₂ according to Eq. (3), with the fugacity coefficients and liquid molar volumes obtained from PC-SAFT (Tables 2 – 3). The solubility-pressure isotherms for the two polymorphic forms were described by PC-SAFT using the same NAP pure-component parameters and binary interaction parameters with CO₂. The comparison with experimental points (Fig. 7) shows that for pressures up to 200 bar, the modeled solubility lines of both polymorphs are close to each other. The same trend is also observed for the experimental data proving the model accuracy in describing the system for the two polymorphic forms. Moreover, this also proves that Türk and Kaska [4] measured the solubility of NAP form 3, whereas in this work we measured the solubility data of both NAP form 1 and NAP form 3.

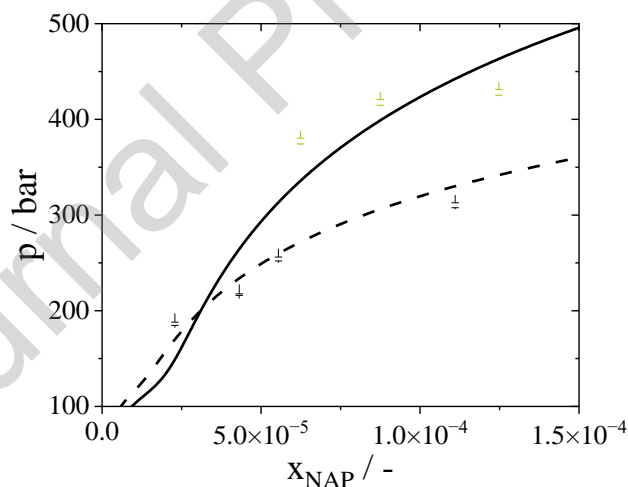


Figure 7. Solubility of NAP in scCO₂ at 60°C. Experimental data are represented by squares [7], triangles [4] and stars (this work). Black stars correspond to NAP form 1, and green stars to NAP form 3, identified in this work. Experimental uncertainties are included for the points measured in this work (stars) but are smaller than the symbols. Solubility lines described by PC-SAFT are represented by dashed line (form 1) and full line (form 3).

4.4. Solubility of IND in scCO₂ and scCO₂/EtOAc mixtures

The experimental results for the solubility of IND in scCO₂ and in scCO₂/EtOAc mixtures are presented in Table 7 and Fig. 8. Table 7 lists the solubility of α -IND in the ternary system as predicted by PC-SAFT for the pressures measured experimentally, whilst Fig. 8b shows PC-SAFT predictions for the average pressures of 150, 250, and 340 bar. Since the difference between the calculated solubilities at the average pressures and the single experimental pressures is not significant, calculated solubilities are plotted for the average pressures in order to keep the diagram clearer to the reader. The solubility of IND in scCO₂ was measured at 60°C in the pressure range of 270 – 390 bar. Due to the extremely low solubility of IND in the supercritical fluid, no sample could be collected from the high-pressure cell after the experiment to perform a PXRD analysis, possibly because all solid was retained within the valve while flushing out the CO₂. However, it is reported in literature that the IND α -form crystal has a higher density compared to the γ -form crystal (1.40 g/cm³ and 1.38 g/cm³, respectively) [41], consequently being the thermodynamic most favorable form under high-pressure conditions [20]. Assuming that the α polymorph was formed at the high pressures applied during the experiments, the melting properties of α -IND, presented in Table 1, were used to calculate the IND solubility in scCO₂, using the parameters from Tables 2 – 3. For the ternary system, the reference pressure was considered to be equal to the system pressure.

Table 7. Experimental solubility data of α -IND measured in this work for the binary system α -IND/scCO₂ and the ternary system α -IND/EtOAc/scCO₂ at $T = 60$ °C, and compared to IND solubilities calculated with PC-SAFT.

Binary system			Ternary system			
p / bar	$x_{\text{IND,exp.}}$	$x_{\text{IND,calc.}}$	p / bar	$x_{\text{EtOAc,IND-free}}$	$x_{\text{IND,exp.}}$	$x_{\text{IND,calc.}}$
272 ± 13	3.22×10^{-5}	2.96×10^{-5}	148 ± 4	0.32	1.75×10^{-3}	1.74×10^{-3}
290 ± 10	3.30×10^{-5}	3.32×10^{-5}	154 ± 4	0.29	1.18×10^{-3}	1.71×10^{-3}
302 ± 9	3.51×10^{-5}	3.53×10^{-5}	159 ± 2	0.20	3.15×10^{-4}	1.27×10^{-3}
321 ± 21	3.74×10^{-5}	3.79×10^{-5}	232 ± 3	0.34	1.93×10^{-3}	1.93×10^{-3}
390 ± 14	4.05×10^{-5}	4.15×10^{-5}	246 ± 5	0.27	1.11×10^{-3}	2.02×10^{-3}
			248 ± 5	0.19	3.77×10^{-4}	1.76×10^{-3}
			341 ± 4	0.40	2.05×10^{-3}	1.83×10^{-3}
			342 ± 9	0.31	1.00×10^{-3}	2.17×10^{-3}
			340 ± 5	0.17	4.33×10^{-5}	2.16×10^{-3}

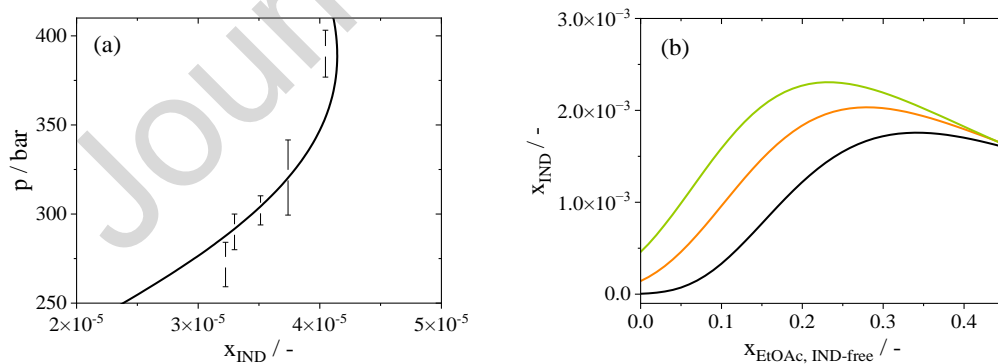


Figure 8. (a) Solubility of α -IND in scCO₂ at 60°C as described by PC-SAFT (line) and measured experimentally in this work (stars). (b) Solubility of α -IND in scCO₂/EtOAc mixtures at 60°C calculated for the average pressures of 150 bar (black), 250 bar (orange), and 340 bar (green). Modeling results using parameters from Tables 2 and 3 are represented by lines and experimental results are indicated as stars.

It can be observed from Table 7 and Fig. 8a that the modeling correctly describes the solubility of α -IND in scCO₂, with a MAD of 2.6×10^{-6} . However, higher deviations between experimental and modeling results are observed for the ternary system (Fig. 8b). In this case, results presented in Table 7 show that the agreement between experimental and calculated solubilities increases with increasing EtOAc concentrations, which also lead to increasing IND solubilities. In contrast, the agreement between experiments and predictions is lowest at low IND solubilities, where the experimental uncertainty is highest. This can be taken as a hint that deviations are mainly caused by experimental uncertainties which of course adds to model limitations. However, the increase in IND solubility with both increasing pressure and increasing EtOAc concentration was correctly described by PC-SAFT including reaching a plateau at higher EtOAc concentrations.

Previous studies also reported an increase in solute solubility with increasing pressures and increasing cosolvent concentrations (for much lower concentrations as used in this work). Ting et al. measured an increasing solubility of NAP with increasing pressure in mixtures of scCO₂ and different organic cosolvents for cosolvent mole fractions up to 0.0525 [7]. Sauceau et al. investigated the solubility of eflucimibe in scCO₂/ethanol and scCO₂/dimethylsulfoxide (DMSO) mixtures at ethanol and DMSO mole fractions of 0.05 and 0.02, respectively [40]. Experimental results showed increasing eflucimibe solubility with increasing pressure for both organic cosolvents. Kopcak et al. reported higher solubilities of caffeine in scCO₂/ethanol and scCO₂/isopropanol at 300 bar compared to 150 bar, at constant cosolvent mole fractions of 0.1 and 0.05 [42].

The solubility of α -IND in the binary mixture scCO₂/EtOAc is two orders of magnitude higher than the solubility in pure scCO₂. This was expected since the addition of an organic

cosolvent to scCO_2 usually increases the density of the mixture, as observed in Fig. 9 for the $\text{scCO}_2/\text{EtOAc}$ binary mixture. Moreover, also the interaction between the API and the cosolvent leads to an additional increase in solubility [43–45].

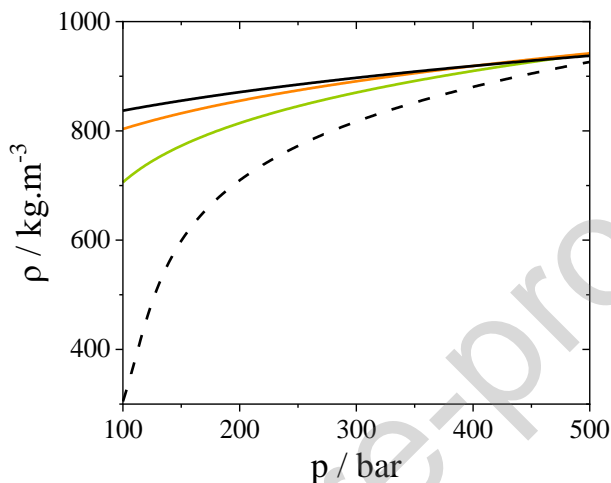


Figure 9 - Density of a $\text{scCO}_2/\text{EtOAc}$ mixture as a function of pressure for $T = 60\text{ }^\circ\text{C}$ and $x_{\text{EtOAc}} = 0$ (dashed), 0.1 (green), 0.2 (orange) and 0.3 (black) as predicted by PC-SAFT.

The increase of a solute solubility in scCO_2 is better illustrated by introducing the cosolvent effect (CE), which is defined as the ratio between the solubility of the API in the mixture $\text{scCO}_2/\text{organic solvent}$ and the one in scCO_2 only. The CE modelled by PC-SAFT for the $\text{IND}/\text{EtOAc}/\text{scCO}_2$ system is presented in Figure 10 for the three different pressures investigated in this work.

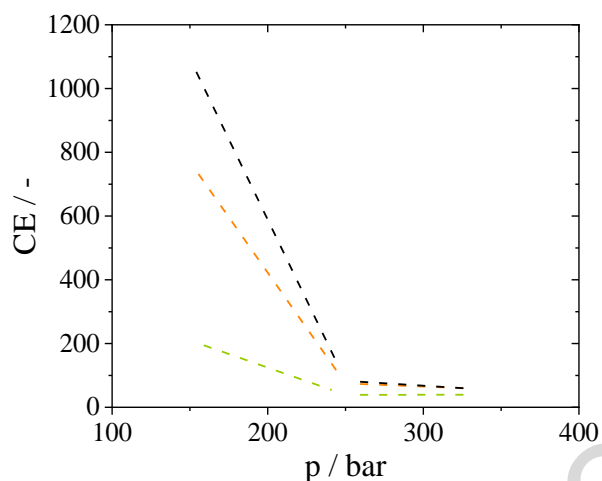


Figure 10 - EtOAc cosolvent effect on IND solubility in $scCO_2$ /EtOAc mixtures as a function of pressure predicted by PC-SAFT at $T = 60\text{ }^\circ\text{C}$ at EtOAc mole fractions in $scCO_2$ of 0.1 (green), 0.2 (orange) and 0.3 (black). CE was calculated for the experimental pressures 150 bar, 250 bar and 340 bar and indicates as circles. Dashed lines are no PC-SAFT calculations but were only inserted to guide the eye.

It can be observed in Fig. 10 that CE decreases with pressure, and the same trend was observed by Ting et al. for systems with NAP [7]. Fig. 10 also depicts an increase in the CE with increasing EtOAc mole fraction in $scCO_2$ for all investigated pressures. However, CE is much higher for the lower investigated pressure of 150 bar, as the relative increase in the $scCO_2$ /EtOAc mixture density compared to the one of pure $scCO_2$ is highest at low pressures, as observed in Fig. 9. As pressure increases, the relative increase in mixture density becomes smaller, and thus its contribution to the CE [44]. The effect of pressure on CE can also be noticed from the experimental results of the ternary system (Fig. 8b), since the solubility of α -IND in $scCO_2$ /EtOAc is not significantly altered with increasing pressure at constant EtOAc concentration.

5. Conclusion

The solubilities of IND and NAP in scCO_2 with and without EtOAc as cosolvent were investigated in this work. A variable-volume high-pressure view cell was used to measure the solubility applying the cloud-point method. The thermodynamic model PC-SAFT was used to describe the solubility of the two APIs in the supercritical fluid mixtures.

The system NAP/ scCO_2 was investigated in order to validate the experimental procedure used in this work. Two different experimental solubility trends were observed, and it was possible to verify by PXRD analysis that different polymorphic forms were obtained, depending on the pressure applied to the system. Pressures above 250 bar favored the transformation of NAP form 1 to NAP form 3. These results suggest that earlier literature data possibly reported the solubility of NAP form 3 in scCO_2 . The different melting properties reported for two NAP polymorphic forms were used for modeling their solubilities in scCO_2 , and PC-SAFT accurately described the NAP solubility in scCO_2 for both polymorphic forms of NAP.

Moreover, the solubility of α -IND in scCO_2 and scCO_2 /EtOAc mixtures was investigated. To the best of our knowledge, this is the first investigation of the solubility of α -IND in scCO_2 at $T = 60\text{ }^\circ\text{C}$, and in scCO_2 /EtOAc mixtures. Modeling results correctly describe the binary system α -IND/ scCO_2 . However, deviations between experimental and modeling results could be observed for the ternary system. This can be attributed to the experimental uncertainties, due to the very low solubility of α -IND in the mixture, as well as to modeling limitations.

Corresponding Author

* Phone: +49 231 755 2635. E-Mail: gabriele.sadowski@tu-dortmund.de

Acknowledgments

This project received funding from the European Union's Horizon 2020 research and innovation program under the Marie Skłodowska-Curie grant agreement No 861278.

Nomenclature

a	Helmholtz energy
A_i, B_i	association sites A and B of molecule i
API	active pharmaceutical ingredient
Δc_p^{SL}	difference in solid and liquid heat capacity
EtOAc	ethyl acetate
f	fugacity
g	Gibbs free energy
h	enthalpy
GLE	gas liquid equilibrium
Δh_{API}^{SL}	API melting enthalpy
IND	indomethacin
k_B	Boltzmann constant
k_{ij}	binary interaction parameter
m_{seg}	segment number
M_w	molecular weight
NAP	naproxen
N^{assoc}	number of association sites

p	pressure
p_c	critical pressure
PC-SAFT	Perturbed-Chain Statistical Associating Fluid Theory
R	universal gas constant
scCO ₂	supercritical carbon dioxide
SLE	solid liquid equilibrium
T	temperature
T_{API}^{SL}	API melting temperature
T_c	critical temperature
u	dispersion energy
v	molar volume
x	mole fraction

Greek characters

ϵ_{AiBi}/k_B	association-energy parameter
μ	chemical potential
ρ	density
κ_{AiBi}	association-volume parameter
σ	segment diameter
φ	fugacity coefficient

Subscripts

calc	calculated
exp	experimental
i, j	component

Superscripts

+	reference
assoc	association
disp	dispersion
F	fluid
G	gas
hc	hard chain
L	liquid
res	residual
S	solid
seg	segment
V	vapor

References

- [1] C. Luebbert, D. Real, G. Sadowski, Choosing Appropriate Solvents for ASD Preparation, *Mol. Pharm.* 15 (2018) 5397–5409. <https://doi.org/10.1021/acs.molpharmaceut.8b00892>.
- [2] M. Perrut, J. Jung, F. Leboeuf, Enhancement of dissolution rate of poorly-soluble active ingredients by supercritical fluid processes: Part I: Micronization of neat particles, *Int. J. Pharm.* 288 (2005) 3–10. <https://doi.org/10.1016/j.ijpharm.2004.09.007>.
- [3] I. Smirnova, M. Türk, R. Wischumerski, M.A. Wahl, Comparison of different methods for enhancing the dissolution rate of poorly soluble drugs: Case of griseofulvin, *Eng. Life Sci.* 5 (2005) 277–280. <https://doi.org/10.1002/elsc.200500081>.
- [4] M. Türk, T. Kraska, Experimental and theoretical investigation of the phase behavior of naproxen in supercritical CO₂, *J. Chem. Eng. Data.* 54 (2009) 1592–1597.

- <https://doi.org/10.1021/je800920d>.
- [5] P. Franco, I. De Marco, Nanoparticles and nanocrystals by supercritical CO₂-assisted techniques for pharmaceutical applications: A review, *Appl. Sci.* 11 (2021) 1–27.
<https://doi.org/10.3390/app11041476>.
- [6] M. Türk, Influence of thermodynamic behaviour and solute properties on homogeneous nucleation in supercritical solutions, *J. Supercrit. Fluids.* 18 (2000) 169–184.
[https://doi.org/10.1016/S0896-8446\(00\)00080-2](https://doi.org/10.1016/S0896-8446(00)00080-2).
- [7] S.S.T. Ting, S.J. Macnaughton, D.L. Tomasko, N.R. Foster, Solubility of Naproxen in Supercritical Carbon Dioxide with and without Cosolvents, *Ind. Eng. Chem. Res.* 32 (1993) 1471–1481. <https://doi.org/10.1021/ie00019a022>.
- [8] A. Garmroodi, J. Hassan, Y. Yamini, Solubilities of the drugs benzocaine, metronidazole benzoate, and naproxen in supercritical carbon dioxide, *J. Chem. Eng. Data.* 49 (2004) 709–712. <https://doi.org/10.1021/je020218w>.
- [9] D. Suleiman, L. Antonio Estévez, J.C. Pulido, J.E. García, C. Mojica, Solubility of anti-inflammatory, anti-cancer, and anti-HIV drugs in supercritical carbon dioxide, *J. Chem. Eng. Data.* 50 (2005) 1234–1241. <https://doi.org/10.1021/je0495511>.
- [10] A.L. Revelli, S. Laugier, A. Erriguible, P. Subra-Paternault, High-pressure solubility of naproxen, nicotinamide and their mixture in acetone with supercritical CO₂ as an anti-solvent, *Fluid Phase Equilib.* 373 (2014) 29–33.
<https://doi.org/10.1016/j.fluid.2014.03.029>.
- [11] L. Padrela, M.A. Rodrigues, J. Tiago, S.P. Velaga, H.A. Matos, E.G. De Azevedo, Insight into the Mechanisms of Cocrystallization of Pharmaceuticals in Supercritical Solvents, *Cryst. Growth Des.* 15 (2015) 3175–3181. <https://doi.org/10.1021/acs.cgd.5b00200>.

- [12] L. Yu, Polymorphism in molecular solids: An extraordinary system of red, orange, and yellow crystals, *Acc. Chem. Res.* 43 (2010) 1257–1266.
<https://doi.org/10.1021/ar100040r>.
- [13] J.S. Song, Y.T. Sohn, Crystal forms of naproxen, *Arch. Pharm. Res.* 34 (2011) 87–90.
<https://doi.org/10.1007/s12272-011-0110-7>.
- [14] M.T. Ruggiero, J.J. Sutton, S.J. Fraser-Miller, A.J. Zaczek, T.M. Korter, K.C. Gordon, J.A. Zeitler, Revisiting the Thermodynamic Stability of Indomethacin Polymorphs with Low-Frequency Vibrational Spectroscopy and Quantum Mechanical Simulations, *Cryst. Growth Des.* 18 (2018) 6513–6520. <https://doi.org/10.1021/acs.cgd.8b00623>.
- [15] S.A. Surwase, J.P. Boetker, D. Saville, B.J. Boyd, K.C. Gordon, L. Peltonen, C.J. Strachan, Indomethacin: New polymorphs of an old drug, *Mol. Pharm.* 10 (2013) 4472–4480. <https://doi.org/10.1021/mp400299a>.
- [16] L. Padrela, M.A. Rodrigues, A. Duarte, A.M.A. Dias, M.E.M. Braga, H.C. de Sousa, Supercritical carbon dioxide-based technologies for the production of drug nanoparticles/nanocrystals – A comprehensive review, *Adv. Drug Deliv. Rev.* 131 (2018) 22–78. <https://doi.org/10.1016/j.addr.2018.07.010>.
- [17] H. Veith, C. Luebbert, G. Sadowski, Correctly Measuring and Predicting Solubilities of Solvates, Hydrates, and Polymorphs, *Cryst. Growth Des.* 20 (2020) 723–735.
<https://doi.org/10.1021/acs.cgd.9b01145>.
- [18] Y. Takebayashi, K. Sue, T. Furuya, S. Yoda, Solubilities of Organic Semiconductors and Nonsteroidal Anti-inflammatory Drugs in Pure and Mixed Organic Solvents: Measurement and Modeling with Hansen Solubility Parameter, *J. Chem. Eng. Data.* 63 (2018) 3889–3901. <https://doi.org/10.1021/acs.jced.8b00536>.

- [19] S. Hellstén, H. Qu, M. Louhi-Kultanen, Screening of Binary Solvent Mixtures and Solvate Formation of Indomethacin, *Chem. Eng. Technol.* 34 (2011) 1667–1674.
<https://doi.org/10.1002/ceat.201100072>.
- [20] T. Okumura, M. Ishida, K. Takayama, M. Otsuka, Polymorphic Transformations of Indomethacin under High Pressures, *J. Pharm. Sci.* 95 (2006) 689–700.
- [21] D.C. Kim, S. Do Yeo, Modification of indomethacin crystals using supercritical and aqueous antisolvent crystallizations, *J. Supercrit. Fluids.* 108 (2016) 96–103.
<https://doi.org/10.1016/j.supflu.2015.10.026>.
- [22] P. Varughese, J. Li, W. Wang, D. Winstead, Supercritical antisolvent processing of γ -Indomethacin: Effects of solvent, concentration, pressure and temperature on SAS processed Indomethacin, *Powder Technol.* 201 (2010) 64–69.
<https://doi.org/10.1016/j.powtec.2010.03.008>.
- [23] Y. Tozuka, Y. Miyazaki, H. Takeuchi, A combinational supercritical CO₂ system for nanoparticle preparation of indomethacin, *Int. J. Pharm.* 386 (2010) 243–248.
<https://doi.org/10.1016/j.ijpharm.2009.10.044>.
- [24] M.A. Rodrigues, J.M. Tiago, A. Duarte, V. Geraldes, H.A. Matos, E. Gomes Azevedo, Polymorphism in Pharmaceutical Drugs by Supercritical CO₂ Processing: Clarifying the Role of the Antisolvent Effect and Atomization Enhancement, *Cryst. Growth Des.* 16 (2016) 6222–6229. <https://doi.org/10.1021/acs.cgd.6b00697>.
- [25] M. Seiler, J. Groß, B. Bungert, G. Sadowski, W. Arlt, Modeling of solid/fluid phase equilibria in multicomponent systems at high pressure, *Chem. Eng. Technol.* 24 (2001) 607–612. [https://doi.org/10.1002/1521-4125\(200106\)24:6<607::AID-CEAT607>3.0.CO;2-T](https://doi.org/10.1002/1521-4125(200106)24:6<607::AID-CEAT607>3.0.CO;2-T).

- [26] R. Paus, Y. Ji, F. Braak, G. Sadowski, Dissolution of crystalline pharmaceuticals: Experimental investigation and thermodynamic modeling, *Ind. Eng. Chem. Res.* 54 (2015) 731–742. <https://doi.org/10.1021/ie503939w>.
- [27] T.E. Daubert, *Physical and Thermodynamic Properties of Pure Chemicals*, 6th ed., Taylor & Francis, 1996.
- [28] J. Gross, G. Sadowski, Perturbed-chain SAFT: An equation of state based on a perturbation theory for chain molecules, *Ind. Eng. Chem. Res.* 40 (2001) 1244–1260. <https://doi.org/10.1021/ie0003887>.
- [29] J.P. Wolbach, S.I. Sandler, Using Molecular Orbital Calculations to Describe the Phase Behavior of Cross-associating Mixtures, *Ind. Eng. Chem. Res.* 37 (1998) 2917–2928. <https://doi.org/https://doi.org/10.1021/ie970781l>.
- [30] A. Prudic, T. Kleetz, M. Korf, Y. Ji, G. Sadowski, Influence of copolymer composition on the phase behavior of solid dispersions, *Mol. Pharm.* 11 (2014) 4189–4198. <https://doi.org/10.1021/mp500412d>.
- [31] A. Tihic, *Group Contribution sPC-SAFT Equation of State*, Technical University of Denmark, 2008.
- [32] S. Schluter, F. Huxoll, K. Grenningloh, G. Sadowski, G. Petzold, M. Bohm, M. Kraume, M. Skiborowski, Unraveling the influence of dissolved gases on permeate flux in organic solvent nanofiltration - experimental analysis, *Sep. Purif. Technol.* (n.d.).
- [33] M. Görnert, G. Sadowski, Phase-equilibrium measurement and modeling of the PMMA/MMA/carbon dioxide ternary system, *J. Supercrit. Fluids.* 46 (2008) 218–225. <https://doi.org/10.1016/j.supflu.2008.02.009>.
- [34] A.P. Kloc, E. Grilla, C.A. Capeletto, M. Papadaki, M.L. Corazza, Phase equilibrium

- measurements and thermodynamic modeling of {CO₂ + diethyl succinate + cosolvent} systems, *Fluid Phase Equilib.* 502 (2019) 112285.
<https://doi.org/10.1016/j.fluid.2019.112285>.
- [35] Y.L. Tian, H.G. Zhu, Y. Xue, Z.H. Liu, L. Yin, Vapor-liquid equilibria of the carbon dioxide + ethyl propanoate and carbon dioxide + ethyl acetate systems at pressure from 2.96 MPa to 11.79 MPa and temperature from 313 K to 393 K, *J. Chem. Eng. Data.* 49 (2004) 1554–1559. <https://doi.org/10.1021/je034224j>.
- [36] S. Sima, V. Feroiu, D. Geană, New high pressure vapor-liquid equilibrium data and density predictions for carbon dioxide+ethyl acetate system, *Fluid Phase Equilib.* 325 (2012) 45–52. <https://doi.org/10.1016/j.fluid.2012.03.028>.
- [37] Y.T. Tsekhanskaya, M.B. Iometev, E. V. Mushkina, Solubility of Naphthalene in Ethylene and Carbon Dioxide under Pressure, *Russ. J. Phys. Chem.* 38 (1964) 1173–1176.
- [38] N.R. Foster, G.S. Gurdial, J.S.L. Yun, K.K. Liong, K.D. Tilly, S.S.T. Ting, H. Singh, J.H. Lee, Significance of the Crossover Pressure in Solid-Supercritical Fluid Phase Equilibria, *Ind. Eng. Chem. Res.* 30 (1991) 1955–1964. <https://doi.org/10.1021/ie00056a044>.
- [39] N.N. Kalikin, R.D. Oparin, A.L. Kolesnikov, Y.A. Budkov, M.G. Kiselev, A crossover of the solid substances solubility in supercritical fluids: What is it in fact?, *J. Mol. Liq.* 334 (2021) 115997. <https://doi.org/10.1016/j.molliq.2021.115997>.
- [40] M. Sauceau, J.J. Letourneau, B. Freiss, D. Richon, J. Fages, Solubility of eflucimibe in supercritical carbon dioxide with or without a co-solvent, *J. Supercrit. Fluids.* 31 (2004) 133–140. <https://doi.org/10.1016/j.supflu.2003.11.004>.
- [41] M. Yoshioka, B.C. Hancock, G. Zografis, Crystallization of indomethacin from the amorphous state below and above its glass transition temperature, *J. Pharm. Sci.* 83 (1994)

- 1700–1705. <https://doi.org/10.1002/jps.2600831211>.
- [42] U. Kopcak, R.S. Mohamed, Caffeine solubility in supercritical carbon dioxide/co-solvent mixtures, *J. Supercrit. Fluids*. 34 (2005) 209–214.
<https://doi.org/10.1016/j.supflu.2004.11.016>.
- [43] J.M. Dobbs, J.M. Wong, R.J. Lahiere, K.P. Johnston, Modification of Supercritical Fluid Phase Behavior Using Polar Cosolvents, *Ind. Eng. Chem. Res.* 26 (1987) 56–65.
<https://doi.org/10.1021/ie00061a011>.
- [44] M.P. Ekart, K.L. Bennett, S.M. Ekart, G.S. Gurdial, C.L. Liotta, C.A. Eckert, Cosolvent interactions in supercritical fluid solutions, *AIChE J.* 39 (1993) 235–248.
<https://doi.org/10.1002/aic.690390206>.
- [45] X. Zhang, B. Han, Z. Hou, J. Zhang, Z. Liu, T. Jiang, J. He, H. Li, Why do co-solvents enhance the solubility of solutes in supercritical fluids? New evidence and opinion, *Chem. - A Eur. J.* 8 (2002) 5107–5111. [https://doi.org/10.1002/1521-3765\(20021115\)8:22<5107::AID-CHEM5107>3.0.CO;2-0](https://doi.org/10.1002/1521-3765(20021115)8:22<5107::AID-CHEM5107>3.0.CO;2-0).

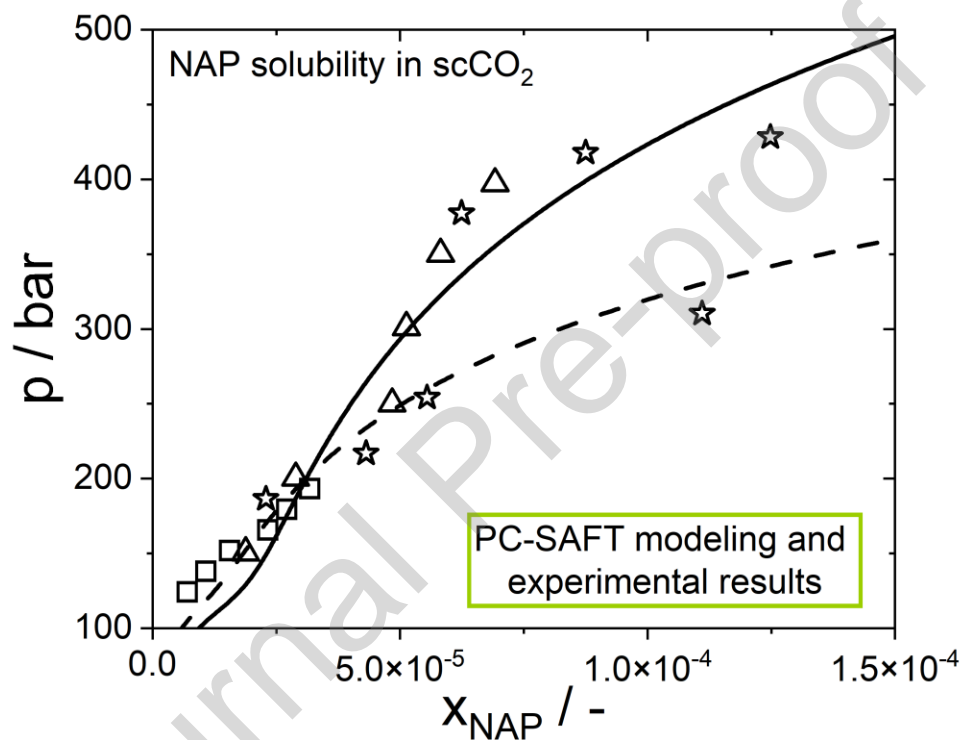
Declaration of interests

The authors declare that they have no known competing financial interests or personal relationships that could have appeared to influence the work reported in this paper.

The authors declare the following financial interests/personal relationships which may be considered as potential competing interests:

Amabelle Petza Kloc reports financial support was provided by EU Framework Programme for Research

Graphical abstract



Highlights

- Pressure applied during solubility measurements affects the solid crystal form of NAP and IND
- EtOAc increases the solubility of IND in scCO₂ by two orders of magnitude
- Cosolvent effect is higher for the lower investigated pressures
- PC-SAFT accurately describes the solubility of different polymorphic forms